Simulation of step input in collective pitch for hovering rotor

Mark A. Woodgate
Research Associate

Thomas A. Fitzgibbon
PhD Student

George N. Barakos
Professor

CFD Laboratory, School of Engineering, University of Glasgow,
Glasgow, G12 8QQ, Scotland, UK

Yongjie Shi
Associate Professor

Pan Li
Associate Professor

National Key Laboratory of Rotorcraft Aeromechanics
Nanjing University of Aeronautics and Astronautics,
Nanjing 210016, China

ABSTRACT

Advanced CFD tools are nowadays used routinely for analysis and design of rotorcraft. Computations for flows around rotors in trim are also common place and slowly the research community is shifting towards simulations of rotorcraft during maneuvering flight. One of the impediments of this effort is the lack of detailed data for validation, evaluation and thorough assessment of CFD methods when it comes to rotors with time-varying inputs. This paper presents a first effort to validate CFD tools for step-inputs in rotor control angles and presents both novel simulations, and un-published experimental data. The results show that there is always a lag involved between the wake and loads response and the operation of low-thrust rotors with dynamic wakes and collective input is a challenging task for modern CFD. The results used in this work originate from a study carried out at the Nanjing University of Aeronautics and Astronautics in China and represent a unique set of great value to the research community. The agreement with simulation results further contributes to the value of the test data.

NOTATION

a	Slope of lift coefficient vs angle of attack (per rad)
c	Blade section chord (m)
F_i	Inviscid flux
F_v	Viscous flux
l	Distance of blade center of mass from flapping hinge, (m)
m_a	Apparent additional mass of air influenced by rotor disk (kg)
m_b	Mass of rotor blades (kg)
M_β	Total flap moment (Nm)
N_b	Number of rotor blades
R	Rotor radius (m)
S	Navier-Stokes equation source term
t	Time (s)
T	Rotor thrust (N)
u, v, w	Velocity components in Cartesian coordinates
v_{ind}	Induced velocity (m/s)
V	Volume (m^3)
W	vector of conservative variables
β	Blade flap angle (rad)
γ	Lock number
θ	Collective pitch (rad)
θ_r	Radial pitch angle (rad)
ρ	Air density (kgm^{-3})
Ω	Rotor rotational speed (rad/s)

Presented at the VFS 76th Annual Forum & Technology Display, October 6–8, 2020, Virtual.

INTRODUCTION

The rotor wake vortex is a dominant feature of the helicopter flow field and it has been identified as one of the primary aspects for predicting helicopter aerodynamics and flight performance (Ref. 1). The rotor wake exhibits an overall periodicity state, while it is highly unsteady and aperiodic during transient maneuvers. The unsteadiness arises from the time lag of the wake dynamic response induced by the ramp control inputs, and also by unsteady fuselage motions fluctuations, etc. results in severe oscillatory airloads and helicopter response. The maneuvering capability is key for several helicopter operations and therefore, there has been an increased effort to develop methods and investigate these complex aerodynamic phenomena during maneuvering flight (Ref. 2).

Over the past few decades, researchers have developed many analytical models for rotor or helicopter simulations for steady flight (Refs. 3–11), but some are failed to simulate the inherent

nonlinearities in transient maneuvering that observed in various dynamics response experiments (Refs. 12–14). To achieve this, a common approach is to account for the unsteady effects on the net thrust and moments. Carpenter (Ref. 12) first developed a dynamic extension of momentum theory by introducing an apparent mass term in thrust equation to model the inertia of the air. They investigated the effect of rapid increase in blade-pitch on rotor airloads and inflow. Following this research, several dynamic inflow models were developed and validated (Refs. 2, 15, 16). These models are widely used in flight simulation for their computational efficiency, but they provide no insight into the rotor wake physics. Therefore, these models are limited to applications where the rotor wake interaction is not severe, and only the total rotor performance, namely thrust and power is concerned.

To explicitly take the wake geometry into account, one approach is via the time-marching wake method. In this method no assumptions regarding periodicity of the wake are made, that is allowed to deform under its own influence and external disturbances. Sadler (Ref. 17) predicted the blade loads during steady turn flight by using a free-wake method with an explicit, Euler time-marching scheme. Bhagwat (Ref. 18) [18] extended the Maryland Free Wake analysis and developed a time-accurate free-vortex method by incorporating a second-order, predictor-corrector time-marching algorithm. They applied this methodology to investigate rotor wake response during several idealized maneuvering flight. The results showed that the overshoot in blade loads during transient maneuvering is caused by the dynamics of buildup in wake structure and induced velocity and is not by flow inertia (Ref. 19). In addition to the vortex filament wake models, Brown (Ref. 20) and He (Ref. 8) presented simulation results of rotor dynamic response to rapid change in collective pitch using vorticity transport method, and a viscous vortex particle model, respectively. These methods satisfactorily simulated the wake distortion and its effects, but the non-linearities around blade were not well captured, especially for modern rotors with complex geometry, due to the lift line or lift surface model are usually employed. Also, there are still some approximations and assumptions in predicting the creations, formations and roll-up of the wake vorticity in these methods.

The first-principle based CFD methodology eliminates the requirements of modeling rotor wake and blade airloads. It has gained much attention in recent years, and there is an increasing application in design and analysis of rotorcraft with CFD methodology (Refs. 21–24), but there are very few works in maneuvering flight simulations. In (Refs. 25–28), researchers carried out the simulations of high-g pull-up maneuver, namely UTTAS 11029, from UH -60A flight test using coupling CFD/CSD method. Their results showed that the current method is able to capture the increase in the mean force during the maneuver, but the non-linearities in the normal force time histories were not satisfactorily predicted. The discrepancy may attribute to the poor capture of dynamic stall events of retreating blade, as well as unclear physics governing the stall. These researches also raised a question that if the state-of-the-art CFD technique can perform well in simulating the complex aerodynamic features of the rotor during aggressive maneuvering.

It is difficult to simulate the dynamic response of complete helicopter during maneuvering flight, and therefore as a first step, we start this research from the dynamic response of an isolated rotor to rapid change in collective pitch which is the most fundamental cases include stop input in control. The other purpose of the this paper is to conduct an well-defined, idealized maneuvering flight experiment using the unique test rigid of Nanjing University of Aeronautics and Astronautics. The test provides reliable data for code validation.

NUMERICAL METHOD

Dynamic inflow method

To model the build-up of the inflow during rotor transient motions, a dynamic inflow equation is obtained by using combined momentum and blade element theory (annulus theory) (Ref. 12). Therefore,

$$\begin{aligned} T &= m_a \dot{v}_{\text{ind}} + 2\pi R^2 \rho v_{\text{ind}} \left[v_{\text{ind}} + \frac{2}{3}\dot{\beta} R \right] \\ &= \frac{1}{6} N_b \rho \Omega^2 \, c_e R^2 \left[\theta_r - \frac{3}{2}\frac{c_1}{c_e}\eta \frac{v_{\text{ind}}}{\Omega R} - \frac{\beta}{\Omega} \right] \end{aligned} \tag{1}$$

Where

$$c_e = \frac{\int_0^R c r^2 \mathrm{d}r}{\int_0^R r^2 \mathrm{d}r}, \quad c_1 = \frac{\int_0^R c r \mathrm{d}r}{\int_0^R r \mathrm{d}r}, \quad m_a = 0.637\rho \left[\frac{4}{3}\pi R^3 \right]. \tag{2}$$

m_a is the apparent mass term with the addition of an impermeable circular disk accelerating in a stagnant fluid, where η is a corrected factor for non-uniform inflow.

The blade flap dynamics equation is coupled to the dynamic inflow model to account for the effect of blade flap.

$$\ddot{\beta} + \Omega^2 \beta = \frac{1}{2}\gamma\Omega^2 \left[\frac{c_2}{c_e}\theta - \frac{4}{3}\tau \frac{v_{\text{ind}}}{\Omega R} - \frac{c_2}{c_e}\frac{\beta}{\Omega} \right] \equiv M_\beta \tag{3}$$

Where

$$c_2 = \frac{\int_0^R c r^3 \mathrm{d}r}{\int_0^R r^3 \mathrm{d}r}, \tag{4}$$

and τ is also a correction for non-uniform inflow.

To reduce the equation to first order, equation 3 is rewritten in a matrix form with two variables β and $\dot{\beta}$,

$$\frac{\mathrm{d}}{\mathrm{d}t}\begin{bmatrix} \beta \\ \dot{\beta} \end{bmatrix} = \begin{bmatrix} 0 & 1 \\ -\Omega^2 & 0 \end{bmatrix} \begin{bmatrix} \beta \\ \dot{\beta} \end{bmatrix} + \begin{bmatrix} 0 \\ M_\beta \end{bmatrix} \tag{5}$$

The systems of differential equations 1 and 5, can be solved by numerical methods, if values of θ and Ω are given against time. Then, the thrust can be computed from the time histories of the variables v_{ind}, β and their derivatives,

$$T = m_a \dot{v}_{\text{ind}} + 2\pi R^2 \rho v_{\text{ind}} \left[v_{\text{ind}} + \frac{2}{3}\dot{\beta} R \right] - m_b l \ddot{\beta}, \tag{6}$$

where m_b is the mass of the blades and l is the distance of the blade center of mass from the flapping hinge.

Time-accurate free wake method

The time-accurate free wake method developed in Reference (Ref. 29) is utilized here to perform simulations complementary to CFD and to the model presented in the previous paragraph. A brief description of the time-accurate free wake method is given here for completeness. In this method, the wake vortices are force-free and convect with the local velocity, the motion of each vortex segment is governed by the convection equation

$$\frac{\mathrm{d}r_v}{\mathrm{d}t} = V_v(r_v), \tag{7}$$

where V_v, is the local fluid velocity, it is composed of free-stream velocity and velocity induced by wake system and rotor maneuvers. A partial differential form of equation 7 is usually employed in numerical solutions, and is written as:

$$\frac{\partial r_v(\psi,\zeta)}{\partial \psi} + \frac{\partial r_v(\psi,\zeta)}{\partial \zeta} = \frac{1}{\Omega} V_v(r_v(\psi,\zeta),t). \tag{8}$$

The growth in vortex core radius is then approximated using

$$\frac{\mathrm{d}r_\zeta}{\mathrm{d}t} = 4\alpha\nu\delta. \tag{9}$$

The blade is divided into several segments along its radius and each segment is modeled using the Weissinger-L lifting-surface model (Ref. 29) Figure 1. The bound vortex is fixed at the 1/4-chord line and control points are located at the 3/4-chord stations. The trailed vortex is assumed to be completely rolled up behind the blade, and the trailed vorticity is concentrated at the tip vortex which comprises the far-wake. The vortex strength in near wake is computed from the no-penetration boundary condition at each control point. A Betz-type vortex sheet roll-up model is used to determine the initial conditions for equations 8 and 9 i.e., initial release point and core radius of the tip vortex. A second-order center difference and backward difference schemes with explicit artificial dissipative terms, named as CB2D scheme is adopted to perform the time marching solution. The blade flapping equation 5 is solved using an explicit time integration scheme. At each time step, these three equations are solved in sequence. Additionally, the time-accurate solution starts from the periodic steady-state solution from the relaxation technique to avoid numerical instability.

Computational Fluid Dynamics method (HMB solver)

All calculations were performed using the parallel CFD solver HMB3 (Helicopter Multi Block) (Ref. 30). HMB3 solves the dimensionless 3D Navier-Stokes equations in integral form using the Arbitrary Lagrangian Eulerian (ALE) formulation for time-dependent domains with moving boundaries:

$$S = \frac{\mathrm{d}}{\mathrm{d}t}\int_{V(t)} W dV + \int_{\partial V(t)} [F_i(W) - F_v(W)] \cdot n dS \tag{10}$$

where V is the time dependent control volume, ∂V is the boundary of the control volume, W is the vector of conservative variables $(\rho, \rho u, \rho v, \rho w, \rho E)$, n is the unit vector on the boundary, F_i and F_v are the inviscid and viscous fluxes respectively.

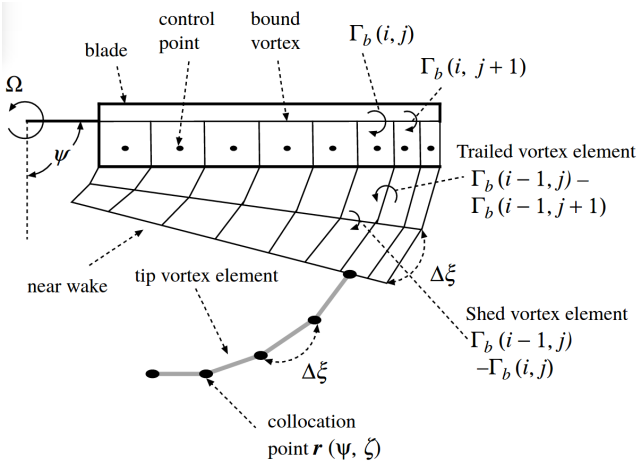

Figure 1. Sketch of the blade model, near wake and tip vortex (Ref. 29).

The Navier-Stokes equations are discretized on the multi-block grid, using a cell-centered finite volume approach. A curvilinear coordinate system is adopted to simplify the formulation of the discretized terms, since body-conforming grids are adopted. The system of equations to be solved is:

$$\frac{\mathrm{d}}{\mathrm{d}t}\left[W_{i,j,k}V_{i,j,k}\right] + R_{i,j,k} = 0. \tag{11}$$

In the above $W_{i,j,k}$ is the vector of conserved variables in the (i,j,k) cell, $V_{i,j,k}$ denotes the volume of the cell and $R_{i,j,k}$ represents the flux residual.

Osher's upwind scheme (Ref. 31) is used to resolve the convective fluxes for its robustness, accuracy and stability properties. The Monotone Upstream-centered Schemes for Conservation Laws (MUSCL) variable extrapolation method is employed in conjunction to formally provide second-order accuracy. The van Albada limiter (Ref. 32) is also applied to remove any spurious oscillations across shock waves. The integration in time is performed with an implicit dual-time method to achieve fast convergence. The linear system is solved using a Krylov subspace algorithm, the generalised conjugate gradient method, with a block incomplete lower-upper (BILU) factorization as a pre-conditioner. The viscous stress tensor is approximated in HMB3 using the Boussinesq hypothesis. The two-equation turbulence model of k-ω has been implemented into flow solver (Ref. 33).

RESULTS AND DISCUSSION

Rotor geometry and mesh

Two model rotors are analyzed in this paper. One is a two-bladed teetering rotor tested in Nanjing University of Aeronautics and Astronautics (NUAA). The rotor has a rectangular and untwisted planform. The blade has a radius of 0.54m, aspect ratio (R/c) of 10 and solidity of 0.0637. The

NACA23012 airfoil is used throughout the blade. The other one is the model rotor tested by Carpenter in 1953 at NACA (Ref. 12). It is a conventional three-blade rotor with flapping hinges located at the center of rotation and drag hinges offset about 0.2286m (9 in) from the center of rotation. The blade radius is 5.8m (19 ft). The blades were made of plywood, were untwisted and had a NACA 23015 airfoil section. The rotor solidity was 0.042. In the literature, only the plan-form view of rotor blades is given, and the blade used in simulation is based on another related paper (Ref. 34). It should be noted that the blade is also not accurately documented, and it is not exactly the same as the one in Carpenter's test. So there are some differences of blade geometry between simulations and tests.

For the blades, a C-topology mesh around the leading edge of the blade was selected, whereas an H-topology was employed at the trailing edge. For hover computations, only a single-blade domain was meshed, assuming periodic conditions for the flow field in the azimuthal direction. This assumption is valid if the wake generated by the rotor is assumed periodic and steady. Table 1 lists the grids employed for this study, showing the main meshing parameters and point distributions over the surface blade. The first cell normal to the blade was set to $8.0 \times 10^{-6}c$ and $1.0 \times 10^{-5}c$ for the NUAA rotor and NACA rotor, respectively, which assures y^+ less than 1.0 all over the blade for the employed Re. A blunt trailing edge was modeled using 42 mesh points. To capture the convection and distortion of tip vortex, the background mesh is refined with the minimize size of 0.03c in the wake development zone. A view of the computational domain along with the employed boundary conditions for hover is given in Figure 2.

Mode	NUAA rotor	NACA rotor
Background mesh size (cells)	19.6 Million	21.8 Million
Blade mesh size (cells)	3.1 Million	3.5 Million
Overall mesh size (cells)	22.7 Million	25.3 Million
Points along the span	171	171
Points around the airfoil	250	250

Table 1. Meshing parameters for the two rotor computational fluid dynamic meshes.

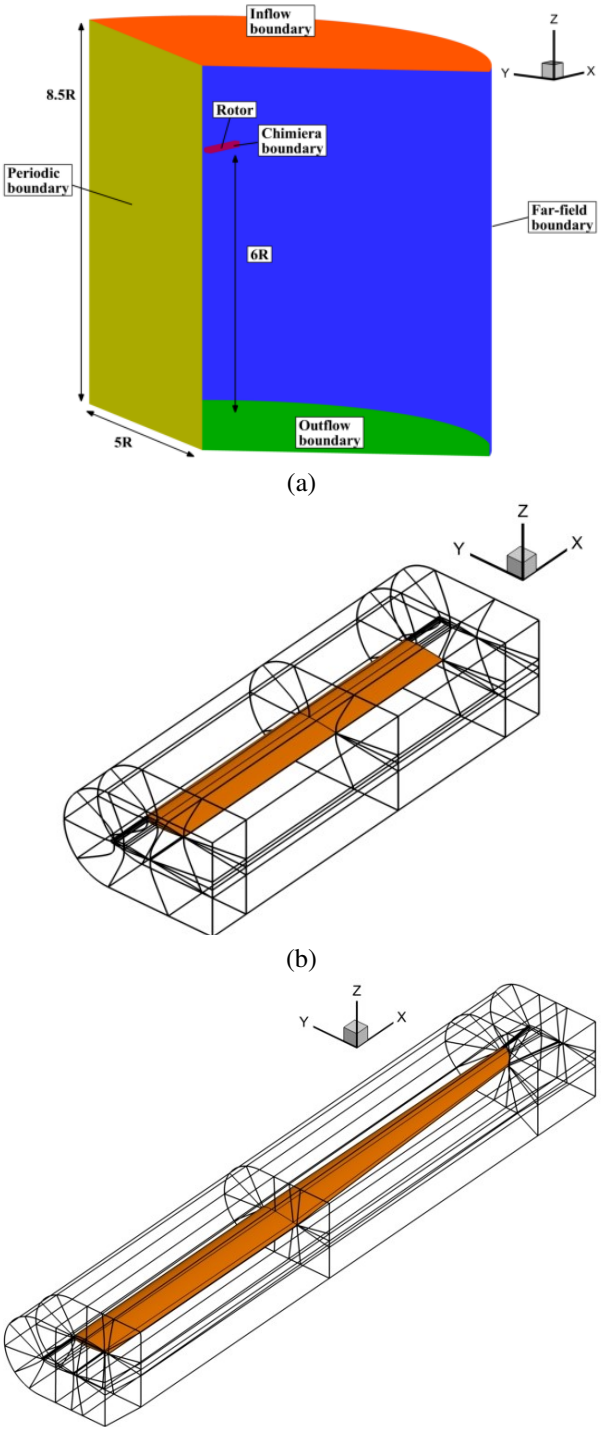

Figure 2. (a) Computational domain and boundary conditions (b) multi-block topology of the NUAA rotor and (c) multi-block topology of the NACA rotor.

Test cases and simulation results

NACA tests

To date, the only available data for validation of methods for cases with ramping rotor collective correspond to the tests by NACA (Ref. 12). Comparisons are show here with our simple dynamic inflow model and these are presented in Figures 3,4,5. One of the key difficulties with the test data is that the blade shape and especially its tip is not fully defined and this makes the case less than ideal for use with CFD tools. The results show that peak of the loads, the time of the thrust peak and the time of the maximum flap angle are not well predicted. In addition, the flap angle values after the peak are also poorly predicted. An important conclusion from the NACA tests is that the slow ramping case of 20 deg/sec shows worst agreement with the model. This justifies the use of a rather low 40 deg/sec case for comparisons using the modern, well-defined data of NUAA as presented.

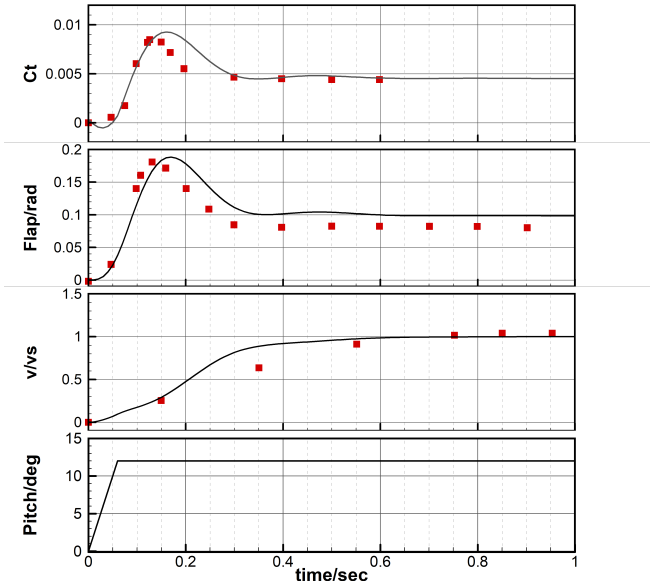

Figure 3. Rapid change of collective pitch at a rate of 200 degrees/sec.

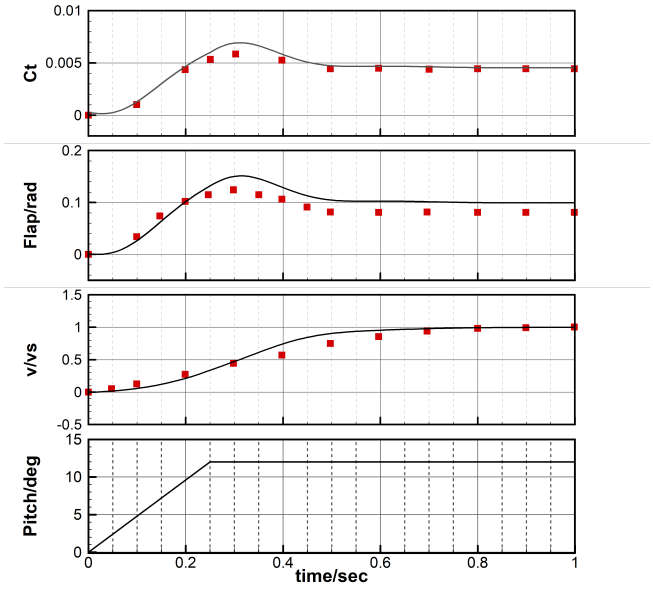

Figure 4. Rapid change of collective pitch at a rate of 48 degrees/sec.

NUAA tests

The experiment of the rotor response to rapid change in control input was carried out using the whirling-beam rotor maneuvering flight test rig of the Nanjing University of Aeronautics and Astronautics. The test rig shown in 6 composes of a rotor system, whirling beam and a pillar. The whirling beam is driven by a servo motor to rotate around the pillar axis. The model rotor was mounted at the end of the whirling beam and could perform rolling and pitching motions through adjusting the horizontal and vertical axis stepper motors. It could also rotate with beam to simulate the forward flight of helicopter. This unique set of experiments by NUAA has a wide range of conditions. The test is conducted using a well-defined blade

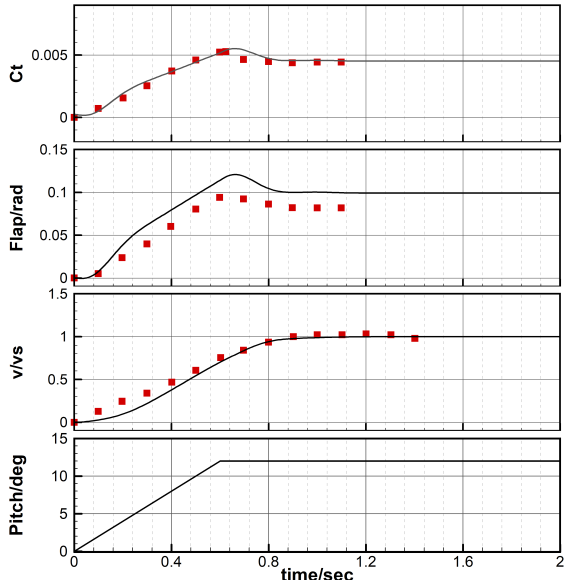

Figure 5. Rapid change of collective pitch at a rate of 20 degrees/sec.

geometry and the result is published in the PH.D thesis by Pan (Ref. 34) in Chinese language. For this reason a description of the test conditions and data obtained is given here.

In this experiment, a series of maneuvering flight tests including the rotor responses to rapid changes in control inputs (collective and cyclic pitches) and angular rate of pitching in hover and forward conditions were carried out. The result of step input in collective pitch is used in this paper. As listed in Table 2, the rotor operates at a rational speed of 1200rpm. The change rate in collective pitch is 40deg/s. The pitch input begins at 0.1s and last for 0.1s too. Three collective settings of 0, 2, and 4 degrees were used.

Parameter	Value
Rotational speed (RPM)	1200
Starting time (sec)	0.1
Duration (sec)	0.1
Initial collective pitch (degrees)	0,2,4
Rate of change of collective pitch (deg/sec)	40

Table 2. Test conditions for the NUAA experiments

Figure 6. The whirling-beam rotor maneuvering flight test rig

The dynamic inflow model used in the previously was also

exercised for this case. Overall the results are in better agreement with the test data and suggest that the NUAA experiments, are somehow easier to reproduce with simulation methods. For all selected values of the initial collective, the CT peak, and the steady-state value after the ramping are well predicted. There is a difference in the times between the collective and load thrust reaching maximum and this suggests that the wake of the rotor may be responding with a delay to the change of the collective.

Figures 7, 8 and 9 plot the experimental and calculation results of the rotor thrust response for three cases. The rapid increase of collectives started at 0.1 seconds and ended at 0.2 seconds. As shown in the figure, the rotor thrust increased linearly during collective input, and reached its maximum value at 0.2 seconds. After that, the thrust began to fluctuate and gradually reached a stable state within 0.5 seconds. The comparisons of three cases shown that the oscillation in thrust is smaller when the initial collective pitch increases. The time-accurate, free-vortex wake model simulated the overshoot and oscillation of the thrust, and predictions correlated well with experimental data.

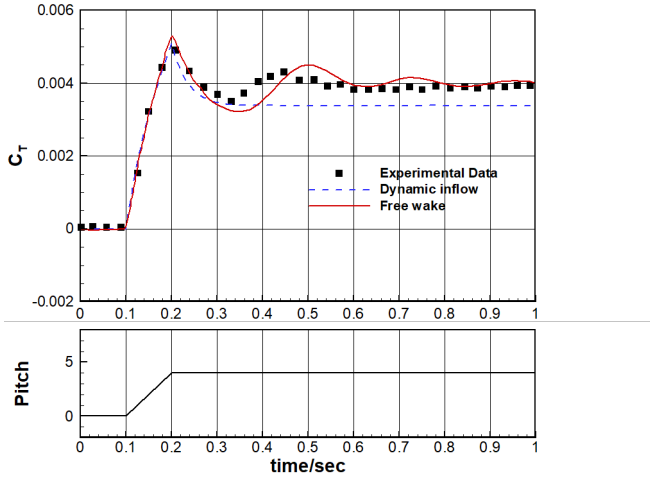

Figure 7. Comparison of the Thrust of the rotor for the NUAA test with initial collective of 0 degrees.

For this teetering rotor, the blades had no rigid flap and the amplitude of elastic flap is small and at high frequency, which had little impact on the time-averaged rotor thrust. Therefore, the overshoot of thrust was mainly caused by the time lag of induced velocity. In dynamic inflow theory, the time lag of induced velocity is modeled by the additional mass of air. From the perspective of vortex theory, it is explained as the generation of wake vorticity and the transport lag behind the changes of collective and thrust.

Figures 10, 11, and 12 show the dynamic response of rotor wake at three initial collectives. Taking the case of 0 degrees as an example, the influence of the wake distortion on rotor thrust is analyzed. The thrust is about zero initially and no wake is generated. Between 0.1s and 0.2s the rotor rotates twice, and two revolutions of wake was generated and enter the flow field, so the induced velocity on the rotor plane is

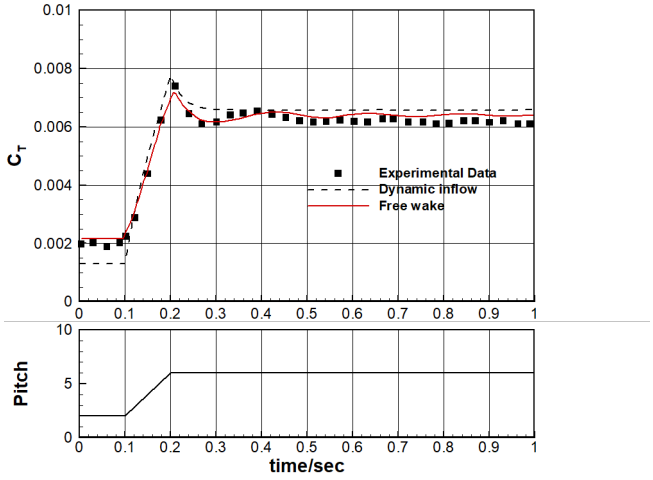

Figure 8. Comparison of the Thrust of the rotor for the NUAA test with initial collective of 2 degrees.

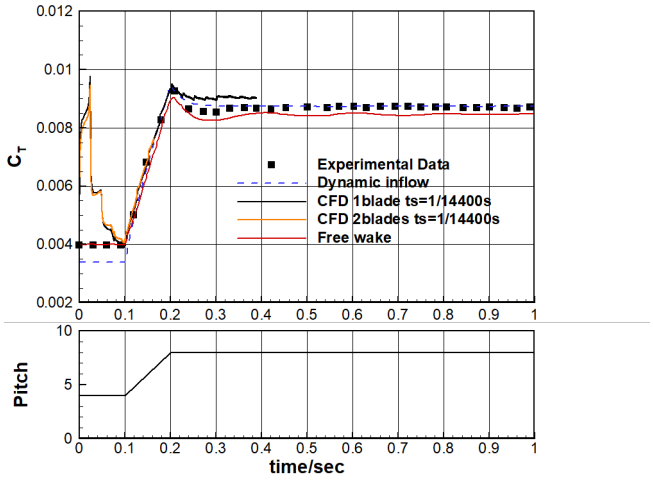

Figure 9. Comparison of the Thrust of the rotor for the NUAA test with initial collective of 4 degrees.

small. After 0.2 seconds, the collective input ends, and the ever-growing wake enters the flow field and intertwines with the preceding wake, forming a vortex ring with concentrated vorticity and moving downstream. The continuous accumulation of vorticity increases the induced velocity at the rotor plane, resulting in a decrease of thrust. With the combined effect of local- and self-induced velocity, the concentrated vortex ring will form a type of spring-like motion, which causes the fluctuation of induced velocity and thrust.

Comparing the geometry of the three wakes at same moment, shows that the velocity of new wake vortex leaving the rotor plane and the concentration of vortex relates to the amplitude of collective pitch. The larger initial collective leads to larger velocity and lower vorticity concentration, and makes the oscillation amplitude of the rotor thrust smaller.

CFD Simulations

The CFD simulations employed the HMB3 tool of Glasgow University and focused on the NUAA experiments. Two cases

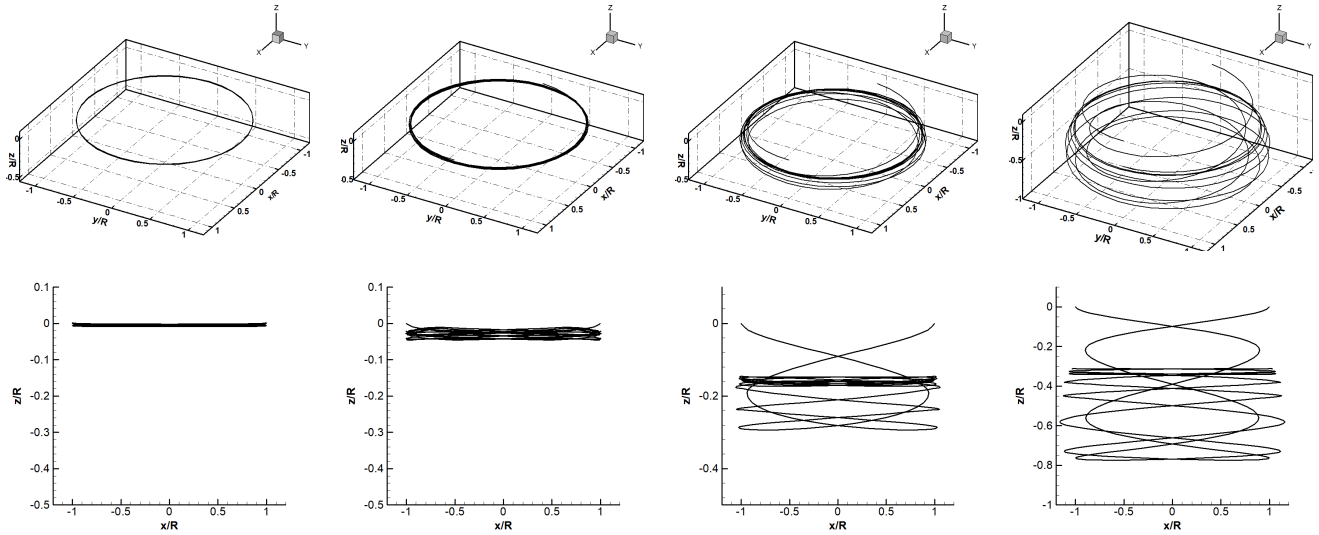

(a) 0.15s (b) 0.2s (c) 0.3s (d) 0.4s

Figure 10. The wake geometry from free-wake simulation with initial collective of 0 degrees.

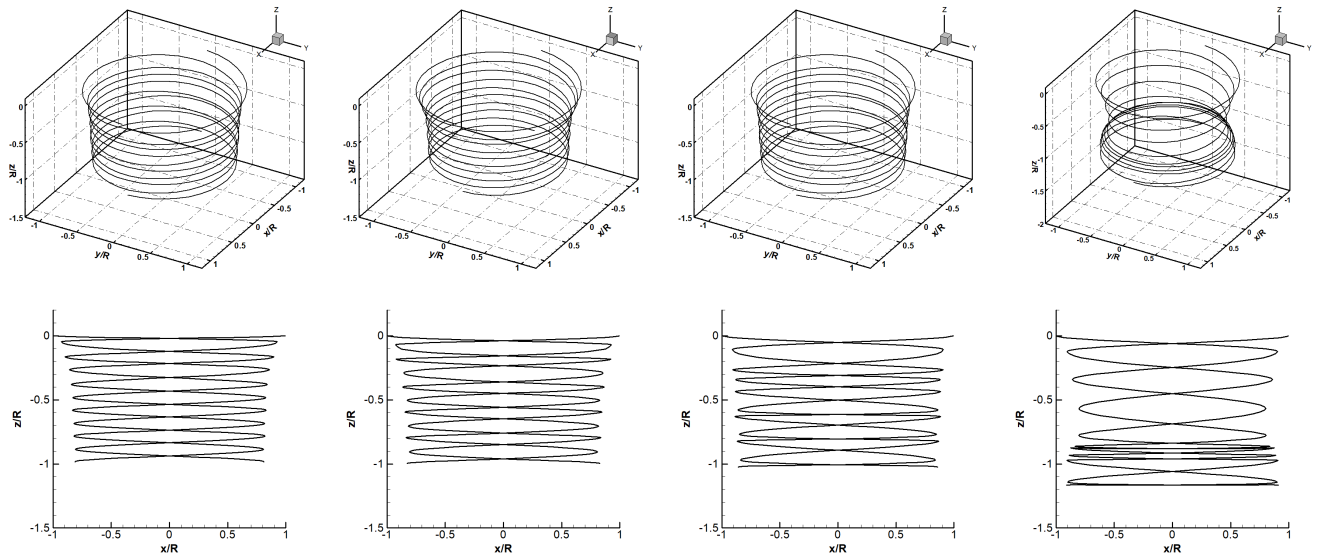

(a) 0.15s (b) 0.2s (c) 0.3s (d) 0.4s

Figure 11. The wake geometry from free-wake simulation with initial collective of 2 degrees.

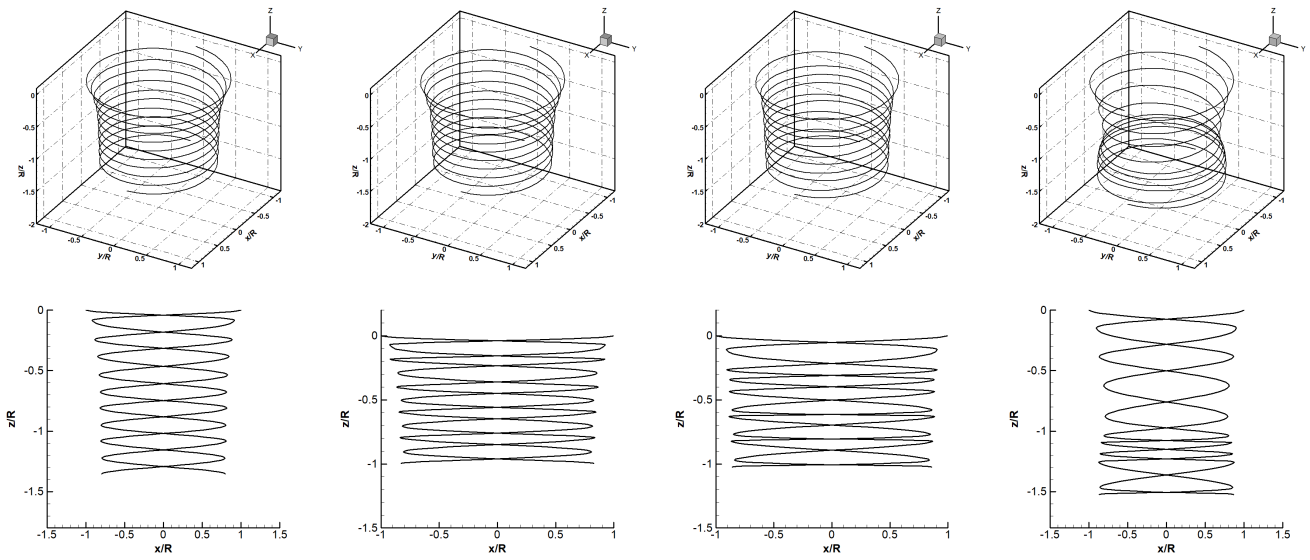

(a) 0.15s (b) 0.2s (c) 0.3s (d) 0.4s

Figure 12. The wake geometry from free-wake simulation with initial collective of 4 degrees.

are considered starting the ramp-up of the rotor from 2 and 4 degrees of collective. The experiments provided detailed time-traces of the collective versus time and the results were approximated using curve-fitting. Figure 9 shows the agreement and the employed polynomials that are given here to allow for exact reproduction of the experimental conditions. The curve-fit employed here is based on a simple method, but this is intentional since the experiment can be reproduced without the need to provide long lists of numbers from the logged history of the rotor collective.

The simulations started with the 4 degree collective case so that the wake is produced by the rotor before the ramping is rather strong, coherent and relatively far from the blade. In addition, the computational domain included only one of the two blades of the rotor. This was mainly done for economy with the computations though a full rotor case with both blades present was also computed. The history of the collective and thrust can be seen in Figure 9 where the flow is seen to converge to the experimental thrust value just before the 0.1 seconds mark. The ramping is relatively fast and the sampling of the experimental signal is rather coarse between 0.1 and 0.2 seconds. The results though of the CFD method appear to track the change of the loads very closely and provide more details in the obtained signal. It is interest to note that the peak thrust value appears ever so slightly later than the peak of the collective. After the peak there is a period of about 0.05 s where the thrust drops before it begins to oscillate with a decreasing amplitude. Steady-state is eventually reached after about 0.4s.

Figure 13 shows visualization of the rotor wake as a function of time. The figure shows a rapidly changing wake that contains the starting vortex of the rotor and the new tip vortex that is changing position and strength due to the variable collective. The thrust of the rotor is rather low and for this reason the wake stays close to the blade and interacts strongly with it. At 0.133s it is clear that the strong initial vortex attracts the tip vortex and since they are co-rotating they wrap around each other. This continues up to 0.155s where the blade begins to produce significant thrust CT $>$ 0.005. Around 0.2 seconds the rotor produces enough thrust to push the initial vortex further below and the results suggest that a rake resembling closer to a rotor in steady hover is reached.

The results for the complete rotor are cross-plotted with the results for the single blade in figure 14 and no significant differences are observed demonstrating the validity of using single-bladed, periodic domain simulations. Both the complete rotor and single bladed simulations had slight blips in the thrust every 180^o when a free-stream initial condition was used. This shows that although using two rotor revolutions converges the thrust to the correct starting value its not enough to remove this transients. It was found that even using 6 and 8 revolutions before the collective pitch-up did not greatly improve the results so another initialization method was used. This method used a fully converged steady state hover calculation as the initial conditions. This removed the small oscillations in the thrust and the recovery of the thrust after the blade has reached 8^o of collective more closely followed the experiment.

Figure 15 shows the position of the vortex cores on a plane 20^o behind the rotor blade as different times. The position of the first core is nearly independent of the collective of the blade. The second core has just moved vertically downwards half way through the collective pitch change. After the collective pitch has reached it maximum the core moved both inboard and farther away from the rotor blade. The third core shows no vertical movement through the first half of collective pitch change but the radial position moves outboard. In the second half of the collective pitch change the core moved away from the rotor blade while reversing direction in the radial direction and finishing up inboard of the initial position. The core has

"overshot" it final position at about time t=0.3s taking another rotor revolution to return close to its final position.

CONCLUSIONS

This work is a first step towards validation of CFD methods for changing inputs to rotors. The experiments of NUAA provide a simple though challenging test case for collective inputs in hover. The results of the CFD are in fair agreement with the test data when refined grids and high temporal resolution was used. The vortex dynamics shows how sensitive the position of the wake is to the initial conditions and its effect on transient response. The vortex dynamics shows some lag between the change in collective input and wake response. The vortex cores settle to an established wake after the collective input is finished but overshoot their positions as the wake adjusts to the changing rotor downwash.

Future work will look further into the wake dynamics and investigate inputs to other rotor control angles.

Author contact:
Woodgate Mark: Mark.Woodgate@glasgow.ac.uk
Fitzgibbon Thomas: t.fitzgibbon.1@research.gla.ac.uk
Barakos George: George.Barakos@glasgow.ac.uk
Shi Yongjie: shiyongjie@nuaa.edu.cn
Li Pan: lipan@nuaa.edu.cn

ACKNOWLEDGMENTS

The sponsorship of the MENtOR (EP/S013814/1) and National Natural Science Foundation of China (No. 11972190) is gratefully acknowledged. This work used the Cirrus UK National Tier-2 HPC Service at EPCC (http://www.cirrus.ac.uk) project ec004 and the ARCHER UK National Supercomputing Service (http://www.archer.ac.uk) project e613.

REFERENCES

1. Komerath, N. M., Smith, M. J., and Tung, C., "A Review of Rotor Wake Physics and Modeling," *Journal of the American Helicopter Society*, Vol. 56, No. 2, 2011, pp. 22006.1–19.

2. Van Hoydonck, W. R. M., Haverdings, H., and Pavel, M. D., "A review of rotorcraft wake modeling methods for flight dynamics applications," *35th European Rotorcraft Forum*, 2009.

3. Drees, J. M., "A theory of airflow through rotors and its application to some helicopter problems," *J. Helicopter Association of Great Britain*, Vol. 3, No. 2, 1949, pp. 79–104.

4. Landgrebe, A. J., "An analytical method for predicting rotor wake geometry," *Journal of the American Helicopter Society*, Vol. 14, No. 4, 1969, pp. 20–32.

5. Bagai, A. and Leishman, J. G., "Rotor Free-Wake Modeling Using a Pseudo-Implicit Technique—Including Comparisons with Experimental Data," *Journal of the American Helicopter Society*, Vol. 40, No. 3, 1995, pp. 29–41.

6. Strawn, R. C. and Caradonna, F. X., "Conservative full-potential model for unsteady transonic rotor flows," *AIAA journal*, Vol. 25, No. 2, 1987, pp. 193–198.

7. Brown, R. E. and Line, A. J., "Efficient high-resolution wake modeling using the vorticity transport equation," *AIAA journal*, Vol. 43, No. 7, 2005, pp. 1434–1443.

8. He, C. and Zhao, J., "Modeling rotor wake dynamics with viscous vortex particle method," *AIAA journal*, Vol. 47, No. 4, 2009, pp. 902–915.

9. Tan, J. F. and Wang, H. W., "Simulating unsteady aerodynamics of helicopter rotor with panel/viscous vortex particle method," *Aerospace Science and Technology*, Vol. 30, No. 1, 2013, pp. 255–268.

10. Ahmad, J. and Duque, E. P., "Helicopter rotor blade computation in unsteady flows using moving overset grids," *Journal of Aircraft*, Vol. 33, No. 1, 1996, pp. 54–60.

11. Shi, Y., Xu, G., and Wei, P., "Rotor wake and flow analysis using a coupled Eulerian–Lagrangian method," *Engineering Applications of Computational Fluid Mechanics*, Vol. 10, No. 1, 2016, pp. 384–402.

12. Carpenter, P. J. and Fridovich, B., "Effect of a rapid blade-pitch increase on the thrust and induced-velocity response of a full-scale helicopter rotor," *NACA TN-3044*, 1953.

13. Ellenrieder, T. and Brinson, P., "The dynamic induced velocity field of a model rotor in hover conditions," *The Aeronautical Journal*, Vol. 102, No. 1016, 1998, pp. 331–336.

14. Jessurun, K., Pavel, M., and Toet, S., "Apparent Mass Effects on a Stiff-Hinged Rotor Model after Rapid Cyclic and/or Collective Inputs-A Flow Visualization Study," *27th European Rotorcraft Forum, Moscow, Russia*, 2001.

15. Pitt, D. M. and Peters, D. A., "Theoretical Prediction of Dynamic – Inflow Derivatives," *Vertica*, Vol. 5, 1981, pp. 21–34.

16. Peters, D. A. and He, C. J., "Finite state induced flow models. II - Three-dimensional rotor disk," *Journal of Aircraft*, Vol. 32, No. 2, 1995, pp. 323–333.

17. Sadler, S. G., "Main rotor free wake geometry effects on blade air loads and response for helicopters in steady maneuvers. Volume 1: Theoretical formulation and analysis of results," *NASA CR-2110*, 1972.

18. Bhagwat, M. J. and Leishman, J. G., "Rotor Aerodynamics During Maneuvering Flight Using a Time-Accurate Free-Vortex Wake," *Journal of the American Helicopter Society*, Vol. 48, No. 3, 2003, pp. 143–158.

19. Bhagwat, M. J. and Leishman, J. G., "Time-accurate free-vortex wake model for dynamic rotor response," *American Helicopter Society Specialist meeting, Atlanta*, 2000.

20. Duraisamy, K. and Brown, R., "Aerodynamic response of a hovering rotor to ramp change in pitch input," *64th American Helicopter Society Annual Forum*, 2008.

21. Strawn, R. C., Caradonna, F. X., and Duque, E. P., "30 years of rotorcraft computational fluid dynamics research and development," *Journal of the American Helicopter Society*, Vol. 51, No. 1, 2006, pp. 5–21.

22. Bhagwat, M. J., Moulton, M. A., and Caradonna, F. X., "Development of a CFD-Based Hover Performance Prediction Tool for Engineering Analysis," *Journal of the American Helicopter Society*, Vol. 52, No. 3, 2007, pp. 175–188.

23. Barakos, G. and Garcia, A. J., "CFD analysis of hover performance of rotors at full-and model-scale conditions," *The Aeronautical Journal*, Vol. 120, No. 1231, 2016, pp. 1386–1424.

24. Duraisamy, K. and Baeder, J. D., "High resolution wake capturing methodology for hovering rotors," *Journal of the American Helicopter Society*, Vol. 52, No. 2, 2007, pp. 110–122.

25. Rajmohan, N., Manivannan, V., Sankar, L., Costello, M., and Bauchau, O., "Development of a Methodology for coupling rotorcraft aeromechanics and vehicle dynamics to study helicopters in maneuvering flight," *AHS 65th Annual Forum*, 2009.

26. Rajmohan, N., *Application of hybrid methodology to rotors in steady and maneuvering flight*, Ph.D. thesis, Georgia Institute of Technology, 2010.

27. Thomas, S., Ananthan, S., and Baeder, J. D., "Wake-coupling CFD-CSD analysis of helicopter rotors in steady and maneuvering flight conditions," *AHS Specialist's Conference on Aeromechanics*, 2010.

28. Bhagwat, M. J., Ormiston, R. A., Saberi, H. A., and Xin, H., "Application of computational fluid dynamics/computational structural dynamics coupling for analysis of rotorcraft airloads and blade loads in maneuvering flight," *Journal of the American Helicopter Society*, Vol. 57, No. 3, 2012, pp. 1–21.

29. Li, P. and Chen, R., "Rotor unsteady aerodynamics model using an efficient free-vortex method," *Aircraft Engineering and Aerospace Technology*, 2012.

30. Steijl, R., Barakos, G., and Badcock, K., "A framework for CFD analysis of helicopter rotors in hover and forward flight," *International Journal for Numerical Methods in Fluids*, Vol. 51, No. 8, 2006, pp. 819–847.

31. Osher, S. and Chakravarthy, S., "Upwind schemes and boundary conditions with applications to Euler equations in general geometries," *Journal of Computational Physics*, Vol. 50, No. 3, 1983, pp. 447–481.

32. Van Albada, G. D., Van Leer, B., and Roberts, W. W., "A comparative study of computational methods in cosmic gas dynamics," *Upwind and high-resolution schemes*, Springer, 1997, pp. 95–103.

33. Menter, F. R., "Two-equation eddy-viscosity turbulence models for engineering applications," *AIAA journal*, Vol. 32, No. 8, 1994, pp. 1598–1605.

34. Li, P., "Rotor unsteady free-vortex wake model and investigation on high-fidelity modeling of helicopter flight dynamics," *Nanjing University of Aeronautics and Astronautics, Nanjing*, 2010.

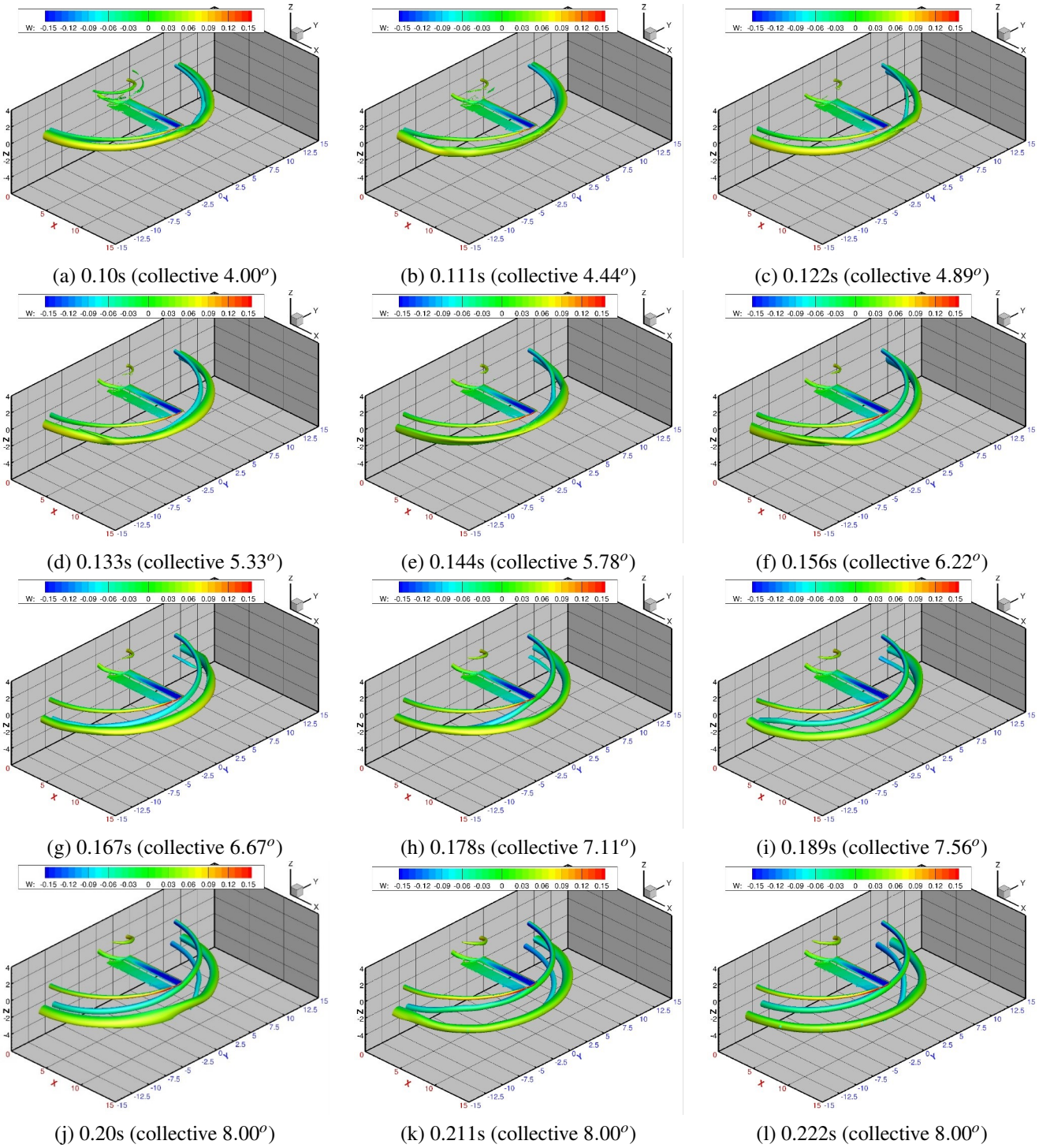

(a) 0.10s (collective 4.00^o) (b) 0.111s (collective 4.44^o) (c) 0.122s (collective 4.89^o)

(d) 0.133s (collective 5.33^o) (e) 0.144s (collective 5.78^o) (f) 0.156s (collective 6.22^o)

(g) 0.167s (collective 6.67^o) (h) 0.178s (collective 7.11^o) (i) 0.189s (collective 7.56^o)

(j) 0.20s (collective 8.00^o) (k) 0.211s (collective 8.00^o) (l) 0.222s (collective 8.00^o)

Figure 13. The wake geometry from CFD simulation with initial collective of 4 degrees.

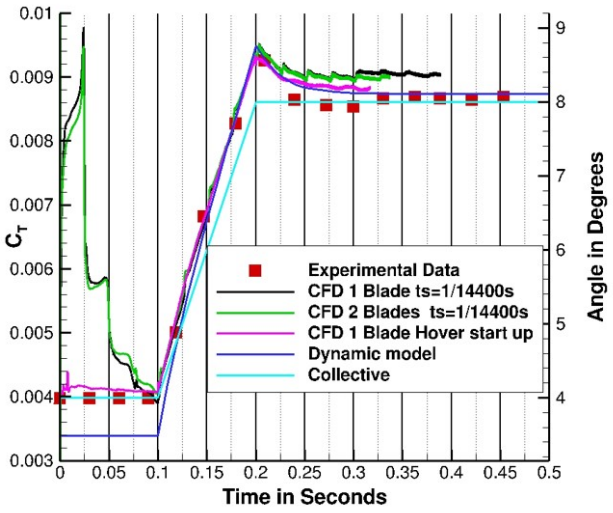

Figure 14. Comparison of the thrust of the rotor for the NUAA test with initial collective of 4 degrees for different CFD configurations.

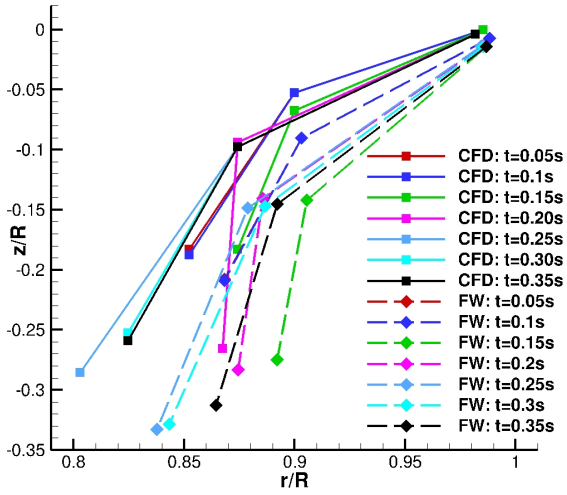

Figure 15. Position of the vortex cores on a plane 20^o behind the rotor blade.